JACS
JOURNAL OF THE AMERICAN CHEMICAL SOCIETY

Article

pubs.acs.org/JACS

Computational Discovery of Picomolar Q_o Site Inhibitors of Cytochrome bc_1 Complex

Ge-Fei Hao,[†,∥] Fu Wang,[†,∥] Hui Li,[†,‡,∥] Xiao-Lei Zhu,[†] Wen-Chao Yang,[†] Li-Shar Huang,[§] Jia-Wei Wu,*[,‡] Edward A. Berry,[§] and Guang-Fu Yang*[,†]

[†]Key Laboratory of Pesticide & Chemical Biology, Ministry of Education, College of Chemistry, Central China Normal University, Wuhan 430079, P. R. China

[‡]MOE Key Laboratory of Protein Sciences, Tsinghua-Peking Center for Life Sciences, School of Life Sciences, Tsinghua University, Beijing 100084, P. R. China

[§]Department of Biochemistry and Molecular Biology, SUNY Upstate Medical University, Syracuse, New York 13210, United States

Supporting Information

ABSTRACT: A critical challenge to the fragment-based drug discovery (FBDD) is its low-throughput nature due to the necessity of biophysical method-based fragment screening. Herein, a method of pharmacophore-linked fragment virtual screening (PFVS) was successfully developed. Its application yielded the first picomolar-range Q_o site inhibitors of the cytochrome bc_1 complex, an important membrane protein for drug and fungicide discovery. Compared with the original hit compound **4** (K_i = 881.80 nM, porcine bc_1), the most potent compound **4f** displayed 20 507-fold improved binding affinity (K_i = 43.00 pM). Compound **4f** was proved to be a noncompetitive inhibitor with respect to the substrate cytochrome *c*, but a competitive inhibitor with respect to the substrate ubiquinol. Additionally, we determined the crystal structure of compound **4e** (K_i = 83.00 pM) bound to the chicken bc_1 at 2.70 Å resolution, providing a molecular basis for understanding its ultrapotency. To our knowledge, this study is the first application of the FBDD method in the discovery of picomolar inhibitors of a membrane protein. This work demonstrates that the novel PFVS approach is a high-throughput drug discovery method, independent of biophysical screening techniques.

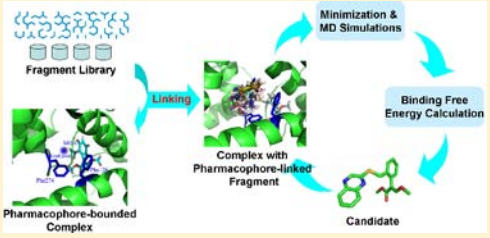

INTRODUCTION

High potency that should be balanced with other properties is a sought-after characteristic of drug molecules. The challenge of discovering high-potency membrane protein inhibitors is of great interest, since about 60% of currently marketed drugs target this type of protein.[1] The cytochrome bc_1 complex (EC 1.10.2.2, bc_1) is an essential and central component of the cellular respiratory chain and of the photosynthetic apparatus in photosynthetic bacteria; it catalyzes the electron transfer (ET) from quinol to a soluble cyt *c*, with concomitant translocation of protons across the membrane to generate a proton gradient and membrane potential for ATP synthesis.[2,3] Its critical importance in life processes makes the bc_1 a promising action target for numerous antiparasitic agents, antibiotics, and fungicides.[4] Three subunits containing prosthetic groups are essential for ET function: the cyt *b* subunit bearing two *b*-type hemes (b_L and b_H heme), cyt c_1 with a *c*-type heme, and the iron−sulfur protein (ISP) having a 2Fe−2S cluster.[5,6] The "proton-motive Q-cycle" is a favored mechanism for electron and proton transfer in this complex,[7] suggesting the existence of two discrete reaction sites: a quinone reduction site near the negative side of the membrane (Q_i or Q_N) and a quinol oxidation site close to the positive side of the membrane (Q_o or Q_P).

Based on inhibition patterns and the crystallographically observed inhibitor binding sites in the bc_1, the existing bc_1 inhibitors can be divided into three classes (Figure 1, Supporting Information):[2] (1) class P inhibitors bind at the Q_o site and include azoxystrobin, kresoxim-methyl, famoxadone, stigmatellin, and UHDBT; (2) class N inhibitors target the Q_i site and include antimycin A and diuron; and (3) class PN inhibitors can bind to both the Q_o and Q_i sites and include NQNO and possibly funiculosin. The most potent bc_1 inhibitor that has been identified is antimycin A, a natural Q_i site inhibitor that binds to bovine heart mitochondrial particles with a dissociation constant of 32 pM.[8] Although Q_o site inhibitors have attracted great interest as antifungal agents, no picomolar range Q_o site inhibitor has yet been reported. Therefore, discovering new ultrapotent Q_o site inhibitors is of great interest, not only for the functional study of bc_1 but also for potential antifungal applications.

Fragment-based drug discovery (FBDD) has recently been rapidly developed as an alternative to traditional methods of hit identification, such as high-throughput screening (HTS).[9] Compared with HTS, FBDD has several significant advantages.[10] First, compared to larger drug-like molecules, fragments

Received: January 13, 2012
Published: June 12, 2012

   dx.doi.org/10.1021/ja3001908 | J. Am. Chem. Soc. 2012, 134, 11168−11176

usually exhibit higher ligand efficiency (LE), which is defined as the binding free energy (ΔG) divided by the heavy atom count (HAC).[11,12] Comparison based on LE rather than potency alone could be useful in determining the potential of drug candidates. Second, the hit rate from fragment screening is typically much higher than that observed with HTS[13] because the property space covered by fragments is much broader and more extensive than that covered by drug-like molecules.[14] Third, in most cases, there are more opportunities to optimize fragments to high quality leads with relatively low molecular weight and better drug-like properties.

However, FBDD also poses challenges. First, FBDD often relies on the detection of fragment binding via sensitive biophysical methods, such as NMR spectroscopy, X-ray diffraction, isothermal calorimetry (ITC), surface plasmon resonance, and mass spectrometry,[15,16] that require specialized equipment, personnel with specific expertise, and supporting informatics infrastructure. Second, due to the much weaker binding affinity of fragments, excellent solubility is required to enable screening at high concentrations. Furthermore, large amounts of purified protein (>10 mg) are always essential, which are very difficult to achieve in most cases, especially for membrane proteins.[17,18] The low-throughput nature of FBDD has prompted several attempts to develop a computational screening method for fragment identification from the much larger commercially available library.[19−21] However, fragment docking is also very challenging; since fragments may be more promiscuous in the binding pocket than larger drug-like molecules, it is very difficult to predict the binding mode of a fragment and accurately estimate its binding affinity.

Based on the X-ray diffraction structures of bc_1 bound to various methoxyacrylate (MOA)-type inhibitors,[2,22] we found that the conformation of the MOA pharmacophore in the binding pocket was highly conserved. This observation prompted us to hypothesize that computational screening of the side-chain fragment without changing the pharmacophore should be an effective way to discover new high-potency bc_1 inhibitors. In the present work, we developed a new approach named pharmacophore-linked fragment virtual screening (PFVS) by integrating the advantages of FBDD and docking methods. Using this new approach, we successfully discovered a series of new bc_1 inhibitors with picomolar potencies. To our knowledge, this is the first application of the FBDD method in the computational discovery of ultrapotent inhibitors of membrane proteins. To verify the simulated binding mode, we also determined the crystal structure of chicken bc_1 in complex with one of the picomolar inhibitors.

RESULTS

Hit Identification through PFVS and Hit Optimization. The workflow of PFVS is shown in Figure 1. During the computational screening, each fragment from a small library containing 1735 fragments was set to link with the MOA pharmacophore via a sulfur atom, since the nucleophilic substitution reaction between the *E*-methyl 2-(2-chloromethylphenyl)-3-methoxyacrylate pharmacophore and the mercapto-containing fragment is highly active and easy to perform. After performing a 3-step computational screening (see the Experimental Section), we obtained 10 hits with the most favorable binding free energies (Table 1, Supporting Information). By setting the criterion of LE over 0.28, five candidates (Figure 2) were selected for chemical synthesis and further evaluation of bc_1 complex−inhibition activity.

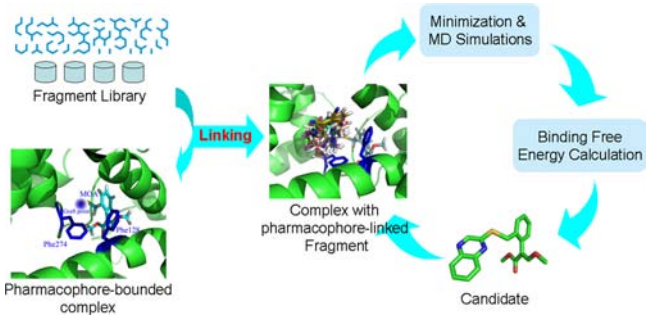

Figure 1. The workflow of PFVS. During the computational virtual screening, each fragment from a small library containing 1735 fragments was set to link with the MOA pharmacophore via a sulfur atom. The energies of the complexes were optimized step by step in a three-step cycle, and candidates were finally determined.

Compound **1** was successfully synthesized but was eventually abandoned because this compound and its *N*-methylated derivatives were determined to be unstable. The synthesis of compound **5** was unsuccessful, but its analogue, **5a**, was obtained with a K_i of 94.97 nM against porcine bc_1. Further optimization of compound **5a** did not significantly improve its potency. We successfully synthesized compounds **2**−**4**, with K_i values against porcine bc_1 of 31.10, 316.09, and 881.80 nM, respectively. Initially, we focused on the structural optimization of the two more prominent compounds, **2** and **3**; however, this did not result in development of a compound with significantly improved potency. Unexpectedly, structural optimization of compound **4**, which contained a side-chain moiety of quinoxaline and exhibited relatively lower inhibitory activity, resulted in several compounds with greatly improved potency (see the following text and Figure 3).

We previously established that improving the Ar−Ar interactions between the side chain of an inhibitor and the hydrophobic residues in the binding pocket (e.g., Phe274) can effectively improve the potency of bc_1 inhibitors.[23] Furthermore, the presence of electron-donating and electron-withdrawing groups can increase the Ar−Ar dimer interaction energies, as can increasing the number of heavy atoms in the dimers.[24] The quinoxalinyl group of compound **4** was surrounded by a hydrophobic pocket formed by the side chains Phe274, Phe127, Ile146, Pro270, Glu271, Ala277, Leu294, Met124, and Ile298 (Figure 4a, numbered according to the cyt *b* subunit of the bovine bc_1). First, we introduced a hydrophobic methyl group onto the 3-position of the quinoxaline ring, creating compound **4a**; this greatly improved the potency (K_i = 41.00 nM) as expected due to the increased Ar−Ar interaction energies between the quinoxalinyl group and its surrounding hydrophobic residues (Figure 4b). Additionally, the LE of compound **4a** was improved to 0.37, higher than that of compound **4** (LE = 0.32). On the other side, we replaced the bridge sulfur atom in compound **4** with an oxygen atom; the resultant compound **4b** also exhibited much higher potency against porcine bc_1 with a K_i value of 51.50 nM and LE of 0.38, which was likely due to the conformational change-induced improvement of the Ar−Ar interaction between the quinoxalinyl ring and the phenyl group of Phe274 (Figure 4c). Combining the above two strategies led to compound **4c** (Figure 4d), whose potency (K_i = 28.00 nM) was further improved. Interestingly, introduction of an additional methyl group onto the 6-position of the quinoxaline ring resulted in

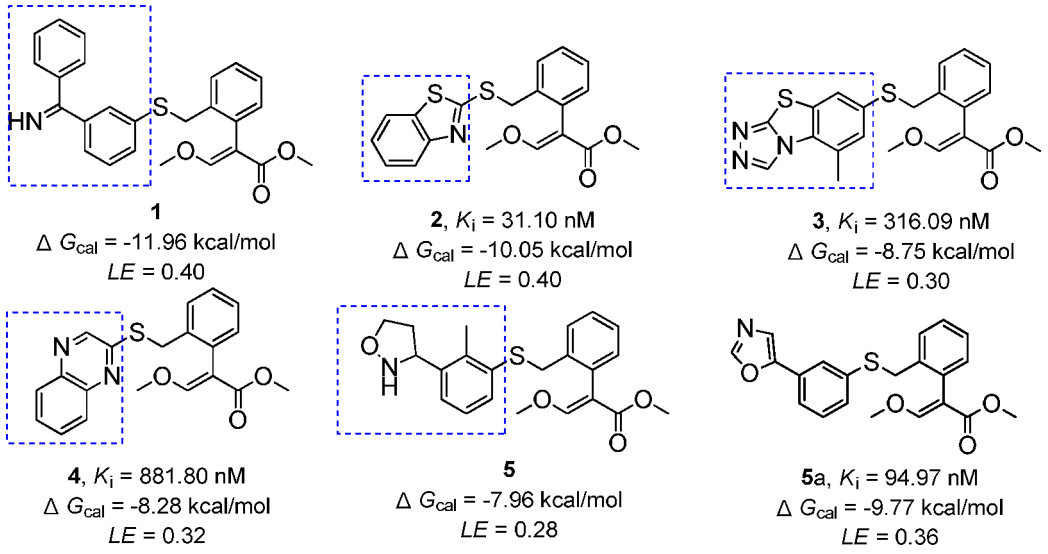

Figure 2. Chemical structures of five final candidates. The fragments determined by PFVS are shown in blue boxes. **5a** is a synthetic analogue of compound **5**. Ligand efficiency (LE) value is defined as the calculated binding free energy (ΔG_{cal}) divided by the HAC, LE = $-\Delta G_{cal}$/HAC.

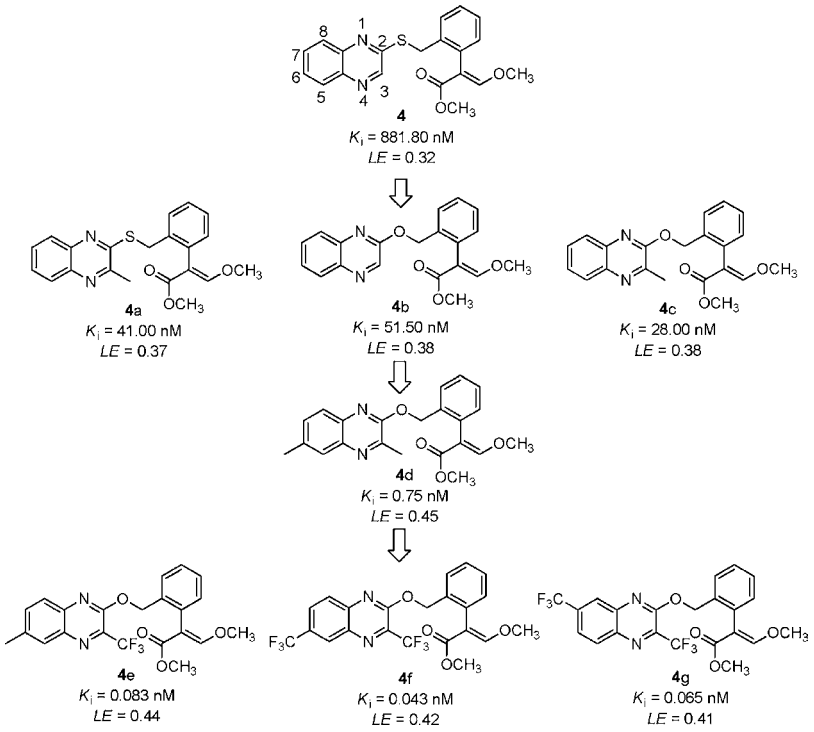

Figure 3. The process of structural optimization of compound **4**. Under the guidance of computational simulation, different fragments were introduced as side-chain moieties onto positions 3, 6, and 7 of quinoxaline; the bridged sulfur atom was also replaced with an oxygen atom. As a result, the potency was improved step by step. Compound **4a** was designed by introducing a hydrophobic methyl group onto the 3-position of the quinoxalinyl ring of compound **4**. Compound **4b** was designed by replacing the bridged sulfur atom with an oxygen atom. Compound **4c** was designed by the combination of the above two strategies. Compound **4d** was designed by introducing an additional methyl group onto the 6-position of compound **4c**. Compound **4e** was designed by replacing the methyl group at the 3-position of compound **4d** with a trifluoromethyl group. Compound **4f** and its isomer **4g** were designed by introducing trifluoromethyl groups to positions 6 and 7 of the quinoxaline ring. The experimentally determined K_i values are marked, and LE values are calculated according to the binding free energies (ΔG_{exp}) derived from K_i values.

compound **4d** (Figure 4e) with a much improved potency (K_i = 0.75 nM).

These results led us to carefully analyze the interactions between the substituted quinoxalinyl ring and its surrounding residues. The methyl group at the 3-position of the quinoxaline ring penetrated into a groove lined by hydrophobic side chains of Pro270, Ile146, Tyr278, and Phe274. Replacing this methyl group with a trifluoromethyl group introduced several C−F···H bonds between the trifluoromethyl and the above-mentioned residues, which is believed to greatly improve the binding free energy.[25] As expected, the resultant compound **4e** formed two C−F···H bonds with Pro270, three with Ile146, and two each with Tyr278 and Phe274; distances between the F and H atoms ranged from 2.45 to 2.98 Å (Figure 4f). The K_i value of

dx.doi.org/10.1021/ja3001908 | J. Am. Chem. Soc. 2012, 134, 11168−11176

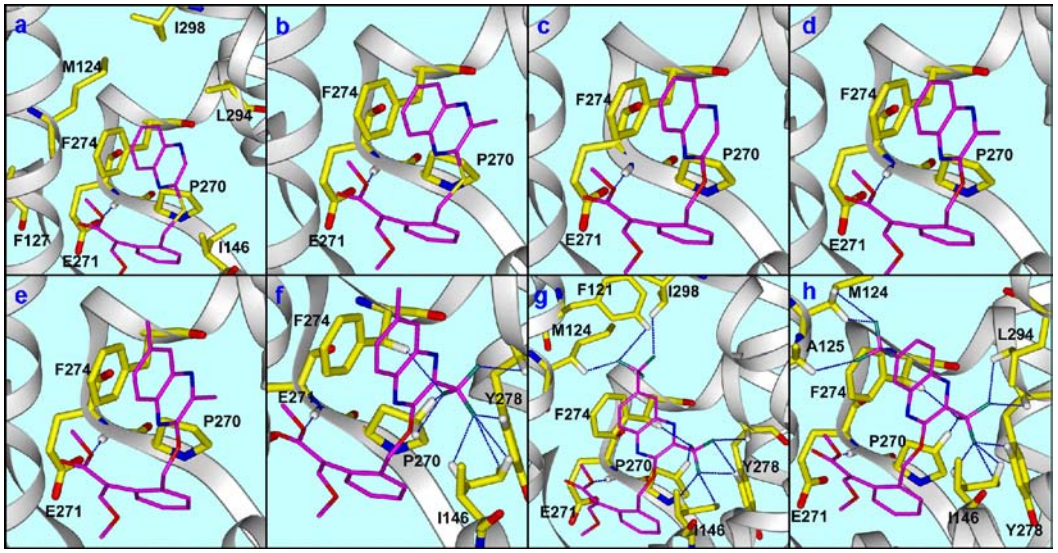

Figure 4. The simulated binding modes of eight different compounds. (a) Side view of the quinoxalinyl group of compound **4** surrounded by a hydrophobic pocket formed by the side chains Phe274, Phe127, Ile146, Pro270, Glu271, Ala277, Leu294, Met124, and Ile298. (b) The potency of compound **4a** is improved greatly due to the improvement of the Ar−Ar interaction energies between the quinoxalinyl group and its surrounding hydrophobic residues. (c) The potency of compound **4b** is improved by the conformational change-induced improvement of the Ar−Ar interaction between the quinoxalinyl ring and the phenyl group of Phe274. (d) The Ar−Ar interaction between the quinoxalinyl ring of compound **4c** and the phenyl group of Phe274 is further improved. (e) The hydrophobic interaction energies between the quinoxalinyl group of compound **4d** and its surrounding hydrophobic residues are further improved. (f) Compound **4e** was designed by replacing the methyl group at position 3 with a trifluoromethyl group, which resulted in two C−F···H bonds with Pro270, three with Ile146, and two each with Tyr278 and Phe274. (g) Additional trifluoromethyl at position 6 of compound **4f** resulted in more C−F···H bonds with F121, M124, and I298. (h) The additional trifluoromethyl at position 7 of compound **4g** resulted in more C−F···H bonds with M124 and A125. The pink lines show the hydrogen and the C−F···H bonds. The F···H distances range from 2.38 to 3.00 Å.

Table 1. Binding Free Energies (kcal/mol) of Compounds 2−4, 4a−g, and 5a

no.	ΔH	$-T\Delta S$	ΔG_{cal}	ΔG_{exp}[a]	K_i (nM)	LE[b]	MW
2	−43.94	33.89	−10.05	−10.26	31.10 ± 0.90	0.41	371.48
3	−40.57	31.82	−8.75	−8.89	316.09 ± 10.71	0.32	411.50
4	−45.74	37.46	−8.28	−8.28	881.80 ± 33.92	0.32	366.44
4a	−49.68	39.63	−10.05	−10.10	41.00 ± 3.60	0.37	380.46
4b	−45.48	36.20	−9.28	−9.97	51.50 ± 1.30	0.38	350.37
4c	−47.45	36.37	−11.08	−10.33	28.00 ± 0.53	0.38	364.39
4d	−48.76	36.47	−12.29	−12.48	0.75 ± 0.23	0.45	378.42
4e	−49.92	37.22	−12.70	−13.78	0.083 ± 0.013	0.44	432.39
4f	−52.55	39.30	−13.25	−14.18	0.043 ± 0.006	0.42	486.36
4g	−51.12	37.96	−13.16	−13.93	0.065 ± 0.018	0.41	486.36
5a	−45.16	35.39	−9.77	−9.60	94.97 ± 3.82	0.36	381.46

[a] $\Delta G_{exp} = -RT\ln K_i$. [b] LE is defined as the experimental binding free energy (ΔG_{exp}) divided by the HAC, LE = $-\Delta G_{exp}$/HAC.

compound **4e** was 0.083 nM, improved 10 624-fold compared to compound **4**; its LE was also greatly increased to 0.44. We further designed two ditrifluoromethyl derivatives, compound **4f** and its isomer, **4g**. As shown in Figure 4g,h, the 6- or 7-position CF_3 group formed several additional C−F···H bonds with the surrounding residues Phe121, Met124, Ile298, and Ala125; the F···H distances ranged from 2.66 to 2.93 Å. The potencies of compounds **4f** and **4g** were further improved 20 507- and 13 566-fold, respectively, compared to the original hit compound **4**; their LE values were still over 0.4. The synthetic routes for compounds **2−4**, **4a−g**, and **5a** are summarized in Scheme 1, Supporting Information. Their chemical structures were characterized by ^{1}H and ^{13}C NMR and HRMS. The crystal structure of compound **4f** (CCDC 831447) was further confirmed by X-ray diffraction analyses (Figure 2, Supporting Information).

It should be noted that the optimization of compound **4** summarized in Figure 3 is based on the above-mentioned computational strategy. The experimental and calculated binding free energies (ΔG) of compounds **2−4**, **4a−g**, and **5a** (Table 1) showed a good linear correlation with a correlation coefficient of r^2 = 0.95, further confirming the reliability of this computational strategy.

Inhibitory Kinetics of Compounds 4 and 4e. Kinetic properties are of great importance for understanding the molecular mechanism of bc_1 function. We therefore examined the inhibitory effects of compounds **4** and **4e** on porcine succinate-cytochrome *c* reductase (SCR, mixture of respiratory complex II and bc_1 complex). As previously described,[23] we measured the complex II activity of SCR using succinate and DCIP as substrates, we used decylubiquinol (DBH_2) and cyt *c* as substrates to measure the bc_1 complex activity, and we used

dx.doi.org/10.1021/ja3001908 | J. Am. Chem. Soc. 2012, 134, 11168−11176

succinate and cyt *c* as substrates to measure SCR (both complex II and bc_1 complex) activity. Both compounds **4** and **4e** significantly inhibited bc_1 complex activity as well as the SCR activity. Neither compound exhibited any effect on the activity of complex II, even with inhibitor concentrations as high as 20 μM. These results indicated that compounds **4** and **4e** are effective bc_1 complex inhibitors.

Compound **4** displayed a linear product versus time relationship (Figure 3, Supporting Information), similar to that of the classical reversible inhibitor azoxystrobin. However, compound **4e** exhibited typical characteristics of a slow, tight-binding inhibitor, with the product formation versus time showing curvilinear functions (Figure 4, Supporting Information). In the presence of compound **4e** and saturated substrate concentrations, the product formation curves started linearly in the initial phase, but the slopes decreased with increasing time, approaching steady states; more dramatic slope reduction was observed with increasing compound **4e** concentrations (Figure 5a). We calculated the observed first-order rate constant (k_{obs}) and found it to be proportional to the concentrations of the inhibitor **4e** (Supporting Information).

Slow-tight binding inhibitors can be further classified as competitive, noncompetitive, or uncompetitive, as ascertained by studying the effect of substrate concentration on k_{obs}. With an increase in the substrate concentration, k_{obs} decreases for a competitive inhibitor, increases for a uncompetitive inhibitor, or is constant for a noncompetitive inhibitor. We next monitored the time courses of bc_1 complex inhibition with different cyt *c* concentrations and a fixed compound **4e** concentration (Figure 5b). The independence of k_{obs} on [cyt *c*] clearly indicated that compound **4e** was a noncompetitive inhibitor with respect to cyt *c*; the inhibition constant can therefore be calculated as $K_i = k_{-0}/k_{+0} = 0.083 \pm 0.013$ nM (Supporting Information).

To assess the effect of the substrate ubiquinol on compound **4e**, we conducted inhibitory kinetic studies of SCR, using DBH_2 and cyt *c* as substrates. In the presence of compound **4e**, the progress curves appeared similarly curvilinear (Figure 6). However, in contrast to the previous observation for cyt *c*, k_{obs} decreased with increasing DBH_2 concentration at a fixed compound **4e** concentration, clearly demonstrating that compound **4e** was a competitive inhibitor with respect to the substrate ubiquinol. To further unravel the inhibitory mechanism, we performed different sets of inhibitory experiments with various concentrations of substrate DBH_2 and inhibitor compound **4e** (Figure 5, Supporting Information). Through detailed kinetic analyses, the inhibition constant K_i was calculated to be 0.974 ± 0.024 nM, approximately 12-fold higher than that derived from the succinate-cyt *c* system. We believe that this discrepancy is largely owing to the presence of the nonionic detergent lauryl maltoside in the assays using DBH_2 as substrate.[23]

Crystal Structure of Chicken bc_1 in Complex with Compound 4e. We determined the crystal structure of the representative compound **4e** bound to chicken bc_1 complex at a resolution of 2.70 Å and found it to be similar to that seen with other MOA-type inhibitors, with the Rieske iron–sulfur protein in the c_1 position.[2] Electron density in the Q_o site (Figure 7a) promoted unambiguous positioning of the inhibitor. As shown in Figure 7b, the pharmacophore of this new inhibitor bound in the fashion of typical MOA inhibitors; the planar methoxyacrylate was inserted into a slot bounded by Phe128, Tyr131, Phe274, and Glu271, with an H-bond between the carbonyl

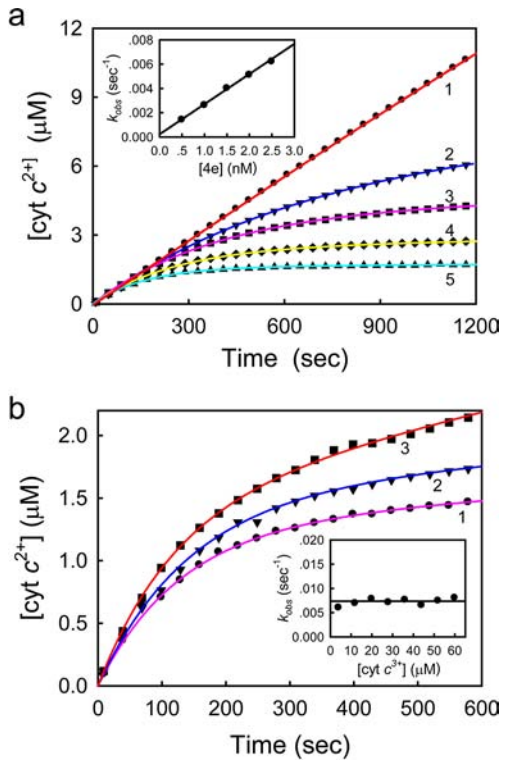

Figure 5. Inhibitory kinetics of bc_1 complex with cyt *c* as substrate by compound **4e.** The enzyme activity was measured using succinate and cyt *c* as substrates. Each reaction mixture contained 100 mM PBS (pH 7.4), 0.3 mM EDTA, 20 mM succinate, and various concentrations of cyt *c* and compound **4e**. The reaction was initiated by adding 0.1 nM SCR to the reaction mixture, and the time course of the absorbance change at 550 nm was recorded continuously for cyt *c* reduction. Experimental data are shown as dots, and theoretical values as lines. (a) Effect of the concentration of **4e** on the inhibition of bc_1 complex. The assays were carried out in the presence of 60 μM of cyt *c* and various concentrations of compound **4e** (1, 0 nM; 2, 0.5 nM; 3, 1 nM; 4, 1.5 nM; and 5, 2.5nM). Inset: Secondary plot of k_{obs} against concentrations of compound **4e**. (b) Effect of cyt *c* concentration on the inhibition of bc_1 complex by compound **4e**. The assays were carried out in the presence of 2 nM of compound **4e** and various concentrations of cyt *c* (1, 20 μM; 2, 28 μM; and 3, 60 μM). Inset: Secondary plot of k_{obs} against concentrations of cyt *c*.

oxygen of the methoxyacrylate and the backbone N of Glu271. The bridging phenyl ring was nearly at right angles to the plane of the methoxyacrylate and was inserted between residues Pro270 and Gly142 (Figure 7c,d). The side chain extended from the bridging ring past the ring of Phe274, in loose contact with Met124, toward an opening to the bulk lipid phase between helices αC and αF. This was presumably the entry path for lipophilic substrates and inhibitors from the lipid phase. The quinoxaline ring stacked with Phe274, and this interaction, predicted by the modeling, has been shown to be important for tight binding. As also predicted by the modeling studies, the trifluoromethyl substituent inserted into a space between Ile146, Phe274, Ala277, and Leu294, capped at the end by Tyr278 (Figure 7c). The fit was quite close, with 10 contacts having less than 3.5 Å between the fluorine atoms and these residues, 4 of them closer than 3.3 Å. While the rotational position of the trifluoromethyl group may not be accurately determined by the data at this resolution, it is clear from the dimensions of the pocket that any rotamer would make numerous contacts.

dx.doi.org/10.1021/ja3001908 | J. Am. Chem. Soc. 2012, 134, 11168–11176

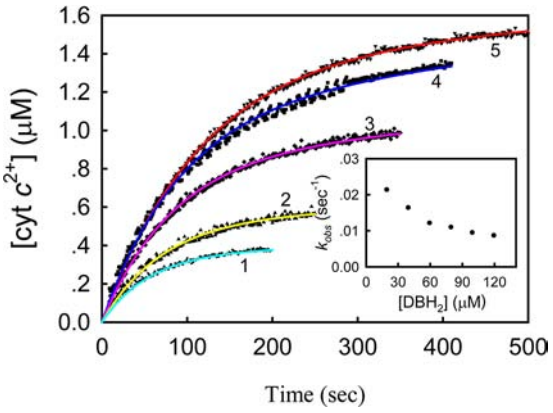

Figure 6. Effect of DBH_2 concentration on the inhibition of bc_1 complex by compound **4e.** The enzyme activity was measured using DBH_2 and cyt *c* as substrates. Each reaction mixture contained 100 mM PBS (pH 6.5), 2 mM EDTA, 750 μM lauryl maltoside, 100 μM oxidized cyt *c*, 20 nM compound **4e**, and various concentrations of DBH_2 (1, 20 μM; 2, 40 μM; 3, 60 μM; 4, 80 μM and 5, 120 μM). Each reaction was initiated by adding 0.05 nM SCR, and the time course of the absorbance change at 550 nm was recorded continuously for cyt *c* reduction. Inset: Secondary plot of k_{obs} against concentration of DBH_2.

Four of the 10 contacts were with Tyr278, and of these, three involved the aromatic side chain. This residue is known to undergo conformational changes depending on the position of the iron–sulfur protein extrinsic domain.[2,26] It is involved in fixing the iron–sulfur protein in the "b" position or famoxadone-induced position,[27] and it may be involved in capturing the iron–sulfur protein from its mobile state. In the presence of MOA inhibitors, Tyr278 formed H-bonds to Ile268 (Figure 7a), partially closing and covering the outward-facing mouth of the Q_o pocket.[26,27] It seems likely that the interactions of Tyr278 with the trifluoromethyl group of the inhibitor stabilized it in this position, preventing it from being released to capture the iron–sulfur protein and thus accounting for the ultrahigh activities of compounds **4e–g**.

The structural similarity between the predicted and the X-ray crystal model was found to be 0.65 Å by assessing the values of the root-mean-square deviation (rmsd) of the atomic positions (Figure 7, Supporting Information), which again confirmed the reliability of our computational protocol. Furthermore, the inhibitor binding of the predicted model was very close to that of the crystal, except for an H-bond in the crystal structure; in the predicted structure, the methoxy rather than carbonyl oxygen of the methoxyacrylate formed an H-bond with the backbone N of Glu271. While this could be a difference between the chicken and the porcine heart bc_1 complexes, structure–activity relationship studies showed that the methoxy oxygen could be replaced by carbon (giving a ketone instead of ester) with little loss of affinity, whereas the carbonyl oxygen was definitely required for any significant affinity.[28] Our previous models may have been unduly influenced by the structure 1SQB used as the starting model; revisiting the modeling results[23] showed that the energetic difference was small. As expected from the modeling studies, the N-containing ring of quinoxaline in the inhibitor side chain stacked with the phenyl ring of Phe274 (Figure 7b).

DISCUSSION

Although FBDD has been widely used in developing new inhibitors against important protein targets, the low-throughput nature of fragment screening continues to raise critical questions about both fundamental and practical aspects of this approach. The present work successfully developed a new PFVS approach, providing a solution to this shortfall of FBDD. When using computational docking for fragment screening, the biggest challenge lies in predicting the binding mode and accurately estimating the binding affinity, due to the promiscuous conformation of a fragment in the binding pocket. However, in our study, when the fragment was linked with the pharmacophore, it became a "drug-like" molecule, making it easy to predict the binding mode and accurately calculate its binding affinity. Using the rational design of bc_1 inhibitors to test our approach, herein, we determined the K_i value of the pharmacophore *E*-methyl-2-(2-methylphenyl)-3-methoxyacrylate to be 4065.12 ± 206 nM, corresponding to a ΔG of −7.37 kcal/mol. Therefore, the contribution of the fragments to the binding free energies of compounds **4a–g** varied from 0.91 to 6.81 kcal/mol. We also estimated the binding energies of the hit fragments of compounds **4a–g**. When keeping the bridge atom invariant except for compounds **4f** and **4g**, the calculated binding energies (ΔH) of these hit fragments were qualitatively consistent with the ΔG values of their corresponding pharmacophore-linked virtual ligands (Figure 8, Supporting Information). Thus, it is practicable to identify the fragment through evaluation of the pharmacophore-linked virtual ligand. Of course, the pharmacophore used in the present work has a highly conserved conformation, which made it much easier to determine the binding mode of the pharmacophore-linked fragments. When using the PFVS approach to design inhibitors of proteins with a conformationally flexible pharmacophore, sufficient energy minimization might be needed to ensure that a rational binding mode will be obtained for the pharmacophore-linked fragments.

Compounds **4e–g**, discovered by PFVS, are the first reported picomolar inhibitors of the bc_1 Q_o site. Compared to that of the original hit compound **4**, the potencies of compounds **4e–g** were improved 10 624-, 20 507-, and 13 566-fold, respectively. The inhibitory kinetics studies showed that these ultrapotent inhibitors exhibited slow-tight binding characteristics, different from those of classical MOA-type inhibitors, such as azoxystrobin and kresoxim-methyl. X-ray crystal diffraction analysis indicated that, although the binding mode of compound **4e** was very similar to that of other MOA-type inhibitors, it involved a unique interaction with residue Tyr278, which constituted a part of the ISP docking crater and was involved in fixing the ISP. It appears that loss of this interaction between Tyr278 and the ISP would induce a more loose state of the ISP extramembrane domain, and it has been established that appropriate ISP mobility is crucial for the catalytic activity of the bc_1 complex. Therefore, a possible explanation of the ultrapotencies of compounds **4e–g** is that, apart from the formation of C–F···H bonds, they enhanced the mobility of the ISP by interacting with residue Tyr278.

In summary, the present promising study shows the newly developed PFVS approach to be a useful tool for the rational design of bc_1 inhibitors. We have demonstrated the use of this approach to yield the first picomolar-range Q_o site inhibitors of the cytochrome bc_1 complex. Furthermore, this high-throughput method is generally applicable to the identification of other types of fragments for drug discovery.

dx.doi.org/10.1021/ja3001908 | J. Am. Chem. Soc. 2012, 134, 11168–11176

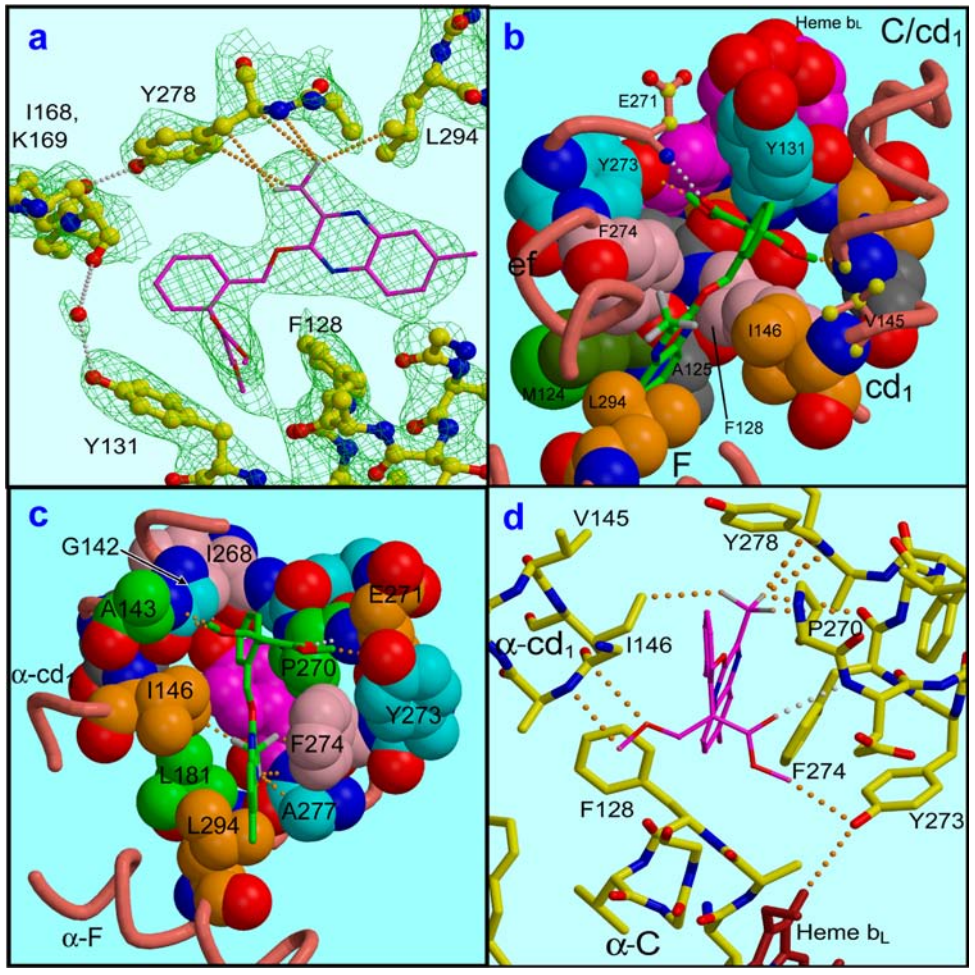

Figure 7. X-ray structure of **4e** bound to chicken bc_1 complex. Residues are numbered according to the bovine/swine sequence. (a) Overall shape of the inhibitor and quality of the electron density (2Fo−Fc map contoured at 1.5 σ). Multiple van der Walls contacts of the trifluoromethyl group with residues 278 and 294 are shown as brown and H-bonds between the residues as white, dotted lines. (b) Space-filling model of the "bottom" of the binding pocket, viewed from above. The inhibitor is shown as a stick figure with green carbons. The pharmacophore, at right angles to the rest of the molecule, fits into a slot at upper right and contacts Glu271, Phe274, and Ala143. The side-chain quinoxaline ring stacks with Phe274. (c) Stick figure model, detailing interactions of the pharmacophore and trifluoromethyl group with the protein. Distances are described in Table 2, Supporting Information. Stereo views of these figures are available in Figure 6, Supporting Information. (d) Space-filling model of the top of the binding pocket, viewed from below. Tyr278 (magenta, unlabeled) blocks the hole in the "top" through which the ISP accesses the site. The phenyl "bridging" ring of the inhibitor inserts between Pro270 and the cd_1 helix at 142−243. The trifluoromethyl group protrudes between Ile146, Phe274, Ala277, and Leu294. Dotted lines show the C−F···H interactions. Both the trifluoromethyl group and the bridging ring make multiple contacts with Tyr278. Stacking of the quinoxaline ring with Phe274 and contacts of the pharmacophore with Glu270, Tyr273, and the cd_1 helix can also be seen.

■ EXPERIMENTAL SECTION

Computational Protocol. The previously established homology model of the porcine bc_1[23] and a small library of 1735 fragments (Supporting Information) were used herein. Because all of the fragments were derived from commercial products in practical use, they should possess good druggable properties that are favorable for de novo design. Based on the modification and combination of AutoGrow and the Amber 8.0 program,[29,30] the PFVS protocol was designed to automatically perform molecule generation, energy minimization, MD simulation, and binding affinity evaluation. The detailed workflow was as follows: (1) The structure of the pharmacophore-binding bc_1 was prepared, and the graft point on the pharmacophore was defined. (2) The fragment was linked to the pharmacophore via a sulfur atom. The orientation of the fragment was minimized to make the minimum steric repulsion with the surrounding residues. (3) The ff99 and gaff parameters for amino acids and ligand were created automatically.[31] (4) Energy minimization and MD simulation were performed on the resultant complex to obtain a reasonable binding conformation. (5) ΔG was calculated as previously described by the combination of the MM/PBSA method[31] for the enthalpy and an empirical method for the entropy.[32]

Fragments were identified by three sequential steps (Figure 9, Supporting Information): (1) All fragments were preliminarily screened. The energy minimization of each newly produced complex was achieved in four steps by using the Sander module of Amber 8.0. First, the fragment was minimized with the pharmacophore and the protein fixed. Then, the ligand was minimized with the protein fixed. Subsequently, the backbone atoms of the protein were fixed, and other atoms were relaxed. The final minimization was performed with both the ligand and the protein relaxed. In each step, the energy minimization was executed by using the steepest descent method for the first 2000 cycles, and the conjugated gradient method for the subsequent 3000 cycles with a convergence criterion of 0.1 kcal mol^{-1} $Å^{-1}$. Then, the ΔH calculation was performed on the minimized complex. To reduce the computational cost, each newly produced ligand was charged by the Gasteiger method, and only the ΔH calculation was considered in the first step. The top ~10% of hits (170) with the most favorable ΔH were selected. (2) These 170 fragments were further estimated by taking the entropy effect into

dx.doi.org/10.1021/ja3001908 | J. Am. Chem. Soc. 2012, 134, 11168−11176

consideration. According to the calculated ΔG, the top-ranked 17 fragments were identified. (3) These 17 virtual ligands were recharged by the restrained electrostatic potential method,[33] then subjected to energy minimization as described in step 1, and additional 20 ps MD simulation. For temperature regulation, the Langevin thermostat was used to maintain a temperature of 300 K.[34] The atomic coordinates were saved per ps. Subsequently, the last snapshot of the MD simulation was minimized to a convergence criterion of 0.1 kcal mol^{-1} $Å^{-1}$. Finally, the ΔG was calculated, and the top-ranked 10 candidates were selected for synthetic evaluation.

Kinetic Assays. The porcine SCR, the mixture of complex II and bc_1, was prepared essentially according to the previously reported method.[35] The enzyme concentration was estimated using an extinction coefficient of 17.5 mM^{-1} cm^{-1} for $A^{552}_{red}-A^{540}_{red}$, which was derived from the cyt c_1 difference spectra between the reduced and oxidized SCR.[36] The three redox reactions are summarized as follows:

$$\text{Assay1: succinate} + \text{cyt } c^{3+} \xrightarrow{\text{SCR}} \text{fumarate} + \text{cyt } c^{2+}$$

$$\text{Assay2: succinate} + \text{DCIP} \xrightarrow{\text{complexII}} \text{fumarate} + \text{DCIPH}_2$$

$$\text{Assay3: DBH}_2 + \text{cyt } c^{3+} \xrightarrow{bc_1\text{complex}} \text{DB} + \text{cyt } c^{2+}$$

The enzymatic activities of SCR, complex II, and the bc_1 complex were analyzed in separate reaction mixtures as reported previously.[37−39] The reactions were initiated by adding a catalytic amount of enzyme to each reaction mixture. The time course of the absorbance change was recorded continuously at 550 nm for cyt c reduction (A^{550}_{red-ox} = 18.5 mM^{-1} cm^{-1}) or 600 nm for DCIP reduction (A^{600}_{red-ox} = 21 mM^{-1} cm^{-1}). Initial rates were determined from the linear slope of the obtained progress curves, and the experimental data were analyzed using a nonlinear regression analysis program.

Crystallization and Structure Determination. Orthorhombic crystals of chicken bc_1 in the space group $P2_12_12_1$, containing a complete dimer in the asymmetric unit, were prepared by sitting-drop vapor diffusion at 273 K, under optimized initial crystallization conditions with 50 mm cacodylate; 9.4 mM TrisHCl; 30 mM K-MES, pH 6.8; 1.8 mM K-MOPS, pH 7.2; 30 mM NaCl; 31 mM KCl; 10 mM $MgCl_2$; 91 g/L glycerol; 30 g/L PEG 4 kDa; 0.9 mM NaN_3; 0.05 mM EDTA; 0.47 g/L undecyl maltoside; and 31 mM octyl glucoside, pH 6.77. Crystals were grown from chicken bc_1 treated with a two-fold excess of **4e**. Diffraction data were collected at beamline A1 of the Cornell High Energy Synchrotron Source (CHESS) at an X-ray wavelength of 0.9770 Å. Data from one crystal extending to 2.70 Å were used to refine the previously determined structure of the protein (3L71), and an electron density map (2Fo−Fc) was calculated. A model of **4e** was placed in the density in the Q_o site map, and the structure including inhibitor was subjected to further rounds of manual rebuilding in O[40] against 2Fo−Fc maps (CCP4)[41] and to automated refinement (atomic positional and individual isotropic ADP) in CNS 1.1.[42] Noncrystallographic symmetry was restrained during positional but not ADP refinement, dividing the monomer into 33 NCS groups and releasing NCS restraints for numerous residues that did not seem to conform to the NCS. As reported in Table 3, Supporting Information, the overall R_{free} value was 0.289 with 0.404 in the last shell justifying the resolution cutoff. Rms deviation from ideal bond lengths (0.008 Å) and angles (1.3°) was reasonable. A total of 85.0% of the residues were within the most favorable region of the Ramachandran plot as defined in the Procheck program,[43] and only 0.3% (nine residues) was in the disallowed region. Four of these (two in each monomer) were known to be "true" outliers from high-resolution structures from a number of species,[44] and three were in poorly ordered regions of subunit 9. The inhibitor and surrounding protein were relatively well ordered, especially in the first monomer (residue C2001), which had an average isotropic ADP of 42.1, well below the average for the protein. The structure and diffraction data have been deposited in the PDB with ID code 3TGU.

■ ASSOCIATED CONTENT

Supporting Information

Chemical compound information. This material is available free of charge via the Internet at http://pubs.acs.org.

■ AUTHOR INFORMATION

Corresponding Author

E-mail: gfyang@mail.ccnu.edu.cn and jiaweiwu@mail.tsinghua.edu.cn

Author Contributions

‖These authors contributed equally.

Notes

The authors declare no competing financial interest.

■ ACKNOWLEDGMENTS

The research was supported in part by the National Basic Research Program of China (no. 2010CB126103) and the NSFC (nos. 20925206, 20932005, and 31070643). We acknowledge Dr. Z. X. Wang for critical discussions and reading of the manuscript. We are also very thankful for the comments and suggestions by anonymous reviewers.

■ REFERENCES

(1) Zheng, C.; Han, L.; Yap, C. W.; Xie, B.; Chen, Y. *Drug Discovery Today* **2006**, *11*, 412−420.
(2) Esser, L.; Quinn, B.; Li, Y. F.; Zhang, M.; Elberry, M.; Yu, L.; Yu, C. A.; Xia, D. *J. Mol. Biol.* **2004**, *341*, 281−302.
(3) Kim, H.; Xia, D.; Yu, C. A.; Xia, J. Z.; Kachurin, A. M.; Zhang, L.; Yu, L.; Deisenhofer, J. *Proc. Natl. Acad. Sci. U.S.A.* **1998**, *95*, 8026−8033.
(4) Barton, V.; Fisher, N.; Biagini, G. A.; Ward, S. A.; O'Neill, P. M. *Curr. Opin. Chem. Biol.* **2010**, *14*, 440−446.
(5) Trumpower, B. L. *J. Bioenerg. Biomembr.* **1991**, *23*, 241−255.
(6) Yang, X. H.; Trumpower, B. L. *Methods Enzymol.* **1986**, *126*, 316−325.
(7) Brandt, U.; Trumpower, B. *Crit. Rev. Biochem. Mol. Biol.* **1994**, *29*, 165−197.
(8) Esser, L.; Elberry, M.; Zhou, F.; Yu, C. A.; Yu, L.; Xia, D. *J. Biol. Chem.* **2008**, *283*, 2846−2857.
(9) Masaya, O.; Masaichi, W.; Yasushi, A.; Kazuki, O.; Tatsuya, N. *Expert Opin. Drug Discovery* **2009**, *4*, 1125−1144.
(10) Murray, C. W.; Rees, D. C. *Nat. Chem.* **2009**, *1*, 187−192.
(11) Hopkins, A. L.; Groom, C. R.; Alex, A. *Drug Discovery Today* **2004**, *9*, 430−431.
(12) Abad-Zapatero, C.; Metz, J. T. *Drug Discovery Today* **2005**, *10*, 464−469.
(13) Hann, M. M.; Leach, A. R.; Harper, G. *J. Chem. Inf. Comput. Sci.* **2001**, *41*, 856−864.
(14) Fink, T.; Bruggesser, H.; Reymond, J. L. *Angew. Chem., Int. Ed.* **2005**, *44*, 1504−1508.
(15) Erlanson, D. A.; McDowell, R. S.; O'Brien, T. *J. Med. Chem.* **2004**, *47*, 3463−3482.
(16) Rees, D. C.; Congreve, M.; Murray, C. W.; Carr, R. *Nat. Rev. Drug Discovery* **2004**, *3*, 660−672.
(17) Fruh, V.; Zhou, Y.; Chen, D.; Loch, C.; Ab, E.; Grinkova, Y. N.; Verheij, H.; Sligar, S. G.; Bushweller, J. H.; Siegal, G. *Chem. Biol.* **2010**, *17*, 881−891.
(18) Congreve, M.; Rich, R. L.; Myszka, D. G.; Figaroa, F.; Siegal, G.; Marshall, F. H. *Methods Enzymol.* **2011**, *493*, 115−36.
(19) Villar, H. O.; Hansen, M. R. *Curr. Top. Med. Chem.* **2007**, *7*, 1509−1513.
(20) Chen, Y.; Shoichet, B. K. *Nat. Chem. Biol.* **2009**, *5*, 358−364.
(21) Lovinge, K.; Alberts, I.; Sherman, W. *Curr. Top. Med. Chem.* **2010**, *10*, 14−32.
(22) Berry, E. A.; Zhang, Z.; Bellamy, H. D.; Huang, L. *Biochim. Biophys. Acta* **2000**, *1459*, 440−448.

(23) Zhao, P. L.; Wang, L.; Zhu, X. L.; Huang, X.; Zhan, C. G.; Wu, J. W.; Yang, G. F. *J. Am. Chem. Soc.* **2010**, *132*, 185−194.
(24) Sanders, J. M. *J. Phys. Chem. A* **2010**, *114*, 9205−9211.
(25) Li, X. Z.; Walker, B.; Michaelides, A. *Proc. Natl. Acad. Sci. U.S.A.* **2011**, *108*, 6369−6373.
(26) Crofts, A. R.; Guergova-Kuras, M.; Kuras, R.; Ugulava, N.; Li, J.; Hong, S. *Biochim. Biophys. Acta, Bioenerg.* **2000**, *1459*, 456−466.
(27) Berry, E. A.; Huang, L.-S. *Biochim. Biophys. Acta, Bioenerg.* **2011**, *1807*, 1349−1363.
(28) Sauter, H.; Ammermann, E.; Roehl, F. *Crop Protection Agents from Nature*; The Royal Society of Chemistry, Thomas Graham House: Cambridge, U.K., 1996.
(29) Durrant, J. D.; Amaro, R. E.; McCammon, J. A. *Chem. Biol. Drug Des.* **2009**, *73*, 168−178.
(30) Case, D. A. et al. *AMBER 8*; University of California: San Francisco, CA, 2004.
(31) Hornak, V.; Abel, R.; Okur, A.; Strockbine, B.; Roitberg, A.; Simmerling, C. *Proteins* **2006**, *65*, 712−725.
(32) Pan, Y.; Gao, D.; Zhan, C. G. *J. Am. Chem. Soc.* **2008**, *130*, 5140−5149.
(33) Cornell, W. D.; Cieplak, P.; Bayly, C. I.; Kollman, P. A. *J. Am. Chem. Soc.* **1993**, *115*, 9620−9631.
(34) Adelman, S. A.; Doll, J. D. *J. Chem. Phys.* **1976**, *64*, 2375−2388.
(35) Yu, L.; Yu, C. A. *J. Biol. Chem.* **1982**, *257*, 2016−2021.
(36) King, T. E. *Methods Enzymol.* **1967**, *10*, 216−225.
(37) Chretien, D.; Slama, A.; Briere, J. J.; Munnich, A.; Rotig, A.; Rustin, P. *Curr. Med. Chem.* **2004**, *11*, 233−239.
(38) Fisher, N.; Bourges, I.; Hill, P.; Brasseur, G.; Meunier, B. *Eur. J. Biochem.* **2004**, *271*, 1292−1298.
(39) Fisher, N.; Brown, A. C.; Sexton, G.; Cook, A.; Windass, J.; Meunier, B. *Eur. J. Biochem.* **2004**, *271*, 2264−2271.
(40) Jones, T. A.; Zou, J. Y.; Cowan, S. W.; Kjeldgaard, M. *Acta Crystallogr. A* **1991**, *47*, 110−119.
(41) Collaborative Computational Project, Number 4. *Acta Crystallogr. Sect. D: Biol. Crystallogr.* **1994**, *50*, 760-763.
(42) Brünger, A. T.; Adams, P. D.; Clore, G. M.; DeLano, W. L.; Gros, P.; Grosse-Kunstleve, R. W.; Jiang, J. S.; Kuszewski, J.; Nilges, M.; Pannu, N. S.; Read, R. J.; Rice, L. M.; Simonson, T.; Warren, G. L. *Acta Crystallogr., Sect. D: Biol. Crystallogr.* **1998**, *54*, 905−921.
(43) Vaguine, A. A.; Richelle, J.; Wodak, S. J. *Acta Crystallogr., Sect. D: Biol. Crystallogr.* **1999**, *55*, 191−205.
(44) Huang, L. S.; Cobessi, D.; Tung, E. Y.; Berry, E. A. *J. Mol. Biol.* **2005**, *351*, 573−597.